Damage localization using experimental modal parameters and topology optimization

Hanno Niemann, Joseph Morlier, Amir Shahdin, Yves Gourinat

Damage Localization using Experimental Modal Parameters and Topology Optimization

Hanno Niemann[a], Joseph Morlier[*,a], Amir Shahdin[a], Yves Gourinat[a]

[a] *Université de Toulouse, Institut Supérieur de l'Aéronatique et de l'Espace, Departement Mécanique des Structures et Matériaux*
BP 54032
10, Ave. Edouard Belin, 31055 Toulouse Cedex 4

Abstract

This work focuses on the developement of a damage detection and localization tool using the Topology Optimization feature of *MSC.Nastran*. This approach is based on the correlation of a local stiffness loss and the change in modal parameters due to damages in structures. The loss in stiffness is accounted by the Topology Optimization approach for updating undamaged numerical models towards similar models with embedded damages. Hereby, only a mass penalization and the changes in experimentally obtained modal parameters are used as objectives. The theoretical background for the implementation of this method is derived and programmed in a *Nastran* input file and the general feasibility of the approach is validated numerically, as well as experimentally by updating a model of an experimentally tested composite laminate specimen. The damages have been introduced to the specimen by controlled low energy impacts and high quality vibration tests have been conducted on the specimen for different levels of damage. These supervised experiments allow to test the numerical diagnosis tool by comparing the result with both NDT technics and results of previous works (concerning shifts in modal parameters due to damage). Good results have finally been archieved for the localization of the damages by the Topology Optimization.

1. Introduction

In recent years the use of fibre composite materials in aeronautical structures has vastly increased. Due to their superior characteristics, concidering e.g. the specific tensile strength, composites are used for a variety of lightweight structures, recently even for pressurized airplane fuselages [1]. Unfortunately, composite structures show a very complex mechanical behavior concerning dynamic loads and a variety of damage mechanisms, that are hard to classify and to predict. Some of these damages are fibre or matrix cracking, fibre matrix debonding and ply delaminations [2].

Composite laminates are susceptible to damages from a wide variety of sources which include fabrication stress, environmental cyclic loading and foreign object impact damage [3]-[5],

[*]Corresponding author. tel: 0033-561-338131
Email addresses: hanno.niemann@tu-bs.de (Hanno Niemann), joseph.morlier@isae.fr (Joseph Morlier), amir.shahdin@isae.fr (Amir Shahdin), yves.gourinat@isae.fr (Yves Gourinat)

and which may lead to severe degradation of the mechanical behavior due to the loss of structural integrity. Therefore, it is even more important to understand the creation and evolution of damages in composites (damage detection), to identify affected regions (damage localization) and to evaluate their influence on the structure as a whole (damage classification and quantification). These steps are the cornerstones of structural health monitoring (SHM) [6]-[8].

In recent years, structural health monitoring using vibration based methods has been rapidly expanding and has shown to be a feasible approach for detecting and locating damage. A detailed and comprehensive overview on the vibration based techniques has been presented in references [7]-[11].

The basic principle of vibration based damage detection can be explained as follows. Any structure can be considered as a dynamic system with stiffness, mass and damping. Once some damages emerge in the structures, the structural parameters will change, and the frequency response functions and modal parameters of the structural system will also change. This change of modal parameters can be taken as the signal of early damage occurrence in the structural system. Vibration-based structural damage detection refers in this context to detection methods for structural damage using only the structural characteristics, such as natural frequencies, modal damping, mode shapes, etc. Structures can be excited by ambient energy, an external shaker or embedded actuators. Accelerometers and laser vibrometers can be used to monitor the structural dynamic responses. A variety of broadband excitation signals have been developed for performing shaker measurements with FFT analyzers, e.g. burst random, burst chirp, etc.. Since the FFT provides a spectrum over a band of frequencies, using a such an excitation signal makes the sprectral measurements much faster than using sine dwell or swept sine excitations [12].

Change in natural frequencies is the most common parameter used in the identification of damaged regions [5],[13]-[17]. Various such methods that use natural frequency information are reported by Salawu [18]. The advantage of using the change of structural natural frequencies to detect damage is its convenient measurement and high accuracy. However the measurement of natural frequencies may not provide enough information for structural damage detection to relate the changes to a correct damage location. Furthermore, natural frequencies are often not sensitive enough to initial damage in structures. Therefore, other damage indicators should also be considered in the damage localization process, like damping or anti-resonances [19].

As listed in [7], several authors have already worked on the idea to correlate damages with a degradation of structural stiffness and/or mass in numerical simulations, which consequently changes the dynamic properties of the numerical model. Adapting this idea, a new approach, using Topology Optimization design variables for localizing damages, has been published [20]. The key of this approach is that, due to the character of Topology Optimization, a search for defects is performed globally over the entire structure, which distinguishes this method from earlier proposed methods and offers interesting prospects.

The original goal of Topology Optimization was to find, within a defined discretized solution domain, a structure of minimal compliance (highest rigidity) by connecting and seperating trusses or insertion and removal of holes in the structure, meaningly by changing the topology. This approach had first been proposed in [21] based on a homogenization of microstructural elements with rectangular holes whose size are defined by the design variable. The dimensions of the holes could vary from 1 (*void*) to 0 (*solid*), normalized to the element's size, and also from element to element. By homogenization of the discrete elements, the composite microstructure could be transformed in an equivalent homogeneous material. Since this method had shown to be rather cumbersome and to deliver hazy results for the optimized structure, a slightly different approach has been presented in [22], which is often referred to as the *Power Law approach*. Here,

the design variables are assumed to be an additional element property that can be understood as a relative density of the element. By reducing the stiffness and mass of certain elements with their newly assigned density fraction property, a local change of structural stiffness and mass can be obtained.

Concerning the damage localization approach, this Topology Optimization variable is now applied to the design domain of a Finite Element model that is based on the undamaged structure. By optimizing the system's stiffness and mass matrix towards those of the damaged structure by matching modal parameters, the correct location and geometry should then theoretically be found in terms of elements with a lower density. In this case, the localization of damage is done by estimating the most probable equivalent damage (local loss of rigidity) which leads to a minimization of the norm between the baseline (undamaged) FRF and experimental FRFs of different damage states. This is the principle idea behind the set up topology optimization formulation for damage localization described in the mentioned article in ref. [20].

In the here presented work, this previous method is implemented in a widely-used commercial code (MSC.Nastran), adding important preliminary tests by computing different Objective functions for fractional mass penalization and validating the results with experimental tests on composites. Thus, from the numerical methodology in [20], we propose a direct application to replace NDE with damage localization by topology optimization with codes, validations and results.

More precisely, in the cited work, the design responses have obviously been calculated using a commercial finite element solver, whereas the topology optimization is performed independently for each iteration loop. The here presented damage localization approach is translated into a Nastran input file, since MSC.Nastran is already equipped with a topology optimization routine as well, which is a supposingly more advanced and more reliant considering the optimization results.

Finally, an experimental validation of the damage localization approach is also tried out on a CFRP specimen by localizing barely visible damage due to low-energy impacts which is an important topic in SHM. At the moment, the diagnostic approach is however still limited on homogeneous isotropic materials due to restrictions in Nastran. Therefore it has been tested on homogenized quasi-isotropic composite beam models. For acquiring the necessary modal data for the damage localisation, vibration tests have been performed on such composite beams. The results offer interesting perspectives considering the damage detection in composite materials and the ultimate goal would be the development of an automatic diagnosis tool as a mean of SHM using only experimental modal data.

2. Numerical Estimation of Modal Parameters

2.1. Mechanical Background

In this section, the theoretical background for the numerical approach used in this work is briefly presented. Basic equations for modal analysis and the calculation of frequency response functions for a discretized system are given. Also, the optimization problems statement for the presented damage localization method is developed.

Eq. 1 shows the set of equations of motion in matrix notation for a random discretized structure. Hereby, the system is considered to be discretized by Finite Elements and $\mathbf{M}$, $\mathbf{C}$ and

K are the system's mass, damping and stiffness matrices, respectively. The vector (f) is a time-dependent load vector.

$$\mathbf{M\ddot{u}} + \mathbf{C\dot{u}} + \mathbf{Ku} = \mathbf{f}(t) \tag{1}$$

The analyses consist of the two principal steps, which are displayed in fig. 1. A modal analysis is performed to determine the principal dynamic characteristics of the system, like natural frequencies and mode shapes. From these modal parameters the response of the structure to excitation can be calculated. This is similar to solving the homogeneous and particular solution for the system of differential equations.

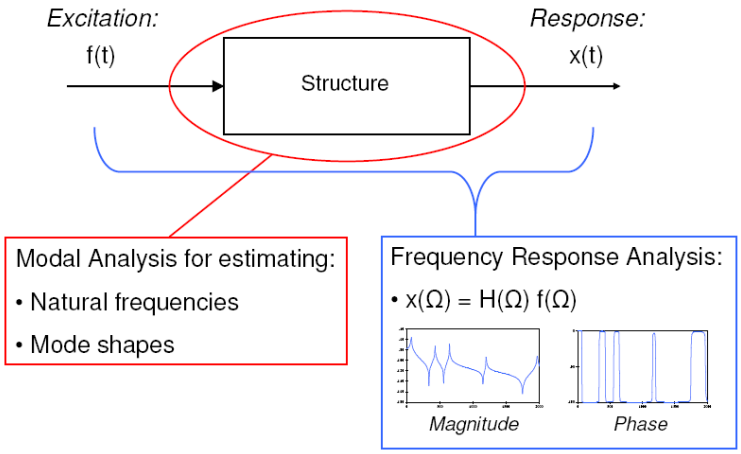

Figure 1: Principal steps of dynamic analyses for structural systems, where **x** is the displacement vector as a response to the excitation force vector **f**. **H** is the matrix of frequency response functions, where Ω is the excitation frequency

2.2. *Modal Analysis*

For calculating the natural frequencies, the system is considered to vibrate harmonically, damping and external forces are neglected. By replacing the displacement vector and its derivative by a sinusoidal solution function, the general eigenvalue problem can be formulated (eq. 2).

$$\left(\mathbf{K} - \omega^2\mathbf{M}\right)\mathbf{u}_0 = 0 \tag{2}$$

Assuming the existence of the vector $\mathbf{u_0}$, meaningly a non-trivial solution of this set of equations, the system's determinant has to vanish. This leads to the *characteristical equation* displayed in eq. 3.

$$\det\left(\mathbf{K} - \lambda\mathbf{M}\right) = 0 \tag{3}$$

The solutions of this equation are the n eigenvalues for a system of n degrees of freedom, where each eigenvalue λ_i corresponds to a natural angular frequency ω_i as stated in eq. 4.

$$\lambda_i = \omega_i^2 \quad \text{with} \quad i = 1, 2, ..., n \tag{4}$$

The amplitude vector corresponding to an eigenvalue is the *eigenvector* or *mode shape vector* $\boldsymbol{\psi}_i$. The combinations of natural frequencies and mode shape vectors describe preferred states of vibration of the structure [23]. For the numerical estimation of the eigenvalues, several algorithms are available, e.g. the *Lanczos method* [24], which is also available in *MSC.Nastran*.

2.3. Modal Frequency Response Analysis (Harmonic Analysis)

The cornerstone of modal frequency response analyses is the diagonalization of the system's matrices by a *modal transformation*. In a seperation approach the primary variables are replaced by a linear combination of the so-called *modal coordinates* and the mode shape vectors, as shown in eq. 5, where $\boldsymbol{\Psi}$ is the *modal matrix* and $\mathbf{q}$ is the vector of modal coordinates.

$$\mathbf{u}(t) = \boldsymbol{\psi}_1 q_1(t) + \boldsymbol{\psi}_2 q_2(t) + ... + \boldsymbol{\psi}_n q_n(t) = \boldsymbol{\Psi}\mathbf{q}(t) \tag{5}$$

Due to the orthogonality properties of the mode shape vectors, inserting the approach into eq. 1 and premultiplying the equation by $\boldsymbol{\Psi}^T$ leads to eq. 6, which are the decoupled equations of motion for the analyzed system. For diagonalizing the damping matrix by the mode shapes vectors from the modal analysis, a *proportional damping approach* [23] has to be assumed.

$$\boldsymbol{\Psi}^T\mathbf{M}\boldsymbol{\Psi}\ddot{\mathbf{q}}(t) + \boldsymbol{\Psi}^T\mathbf{C}\boldsymbol{\Psi}\dot{\mathbf{q}}(t) + \boldsymbol{\Psi}^T\mathbf{K}\boldsymbol{\Psi}\mathbf{q}(t) = \boldsymbol{\Psi}^T\mathbf{f}(t) \tag{6}$$

The system now consists of n equations of motion for *single degree of freedom oscillators* in form of eq. 7, where m_i is the modal mass, c_i a modal damping coefficient, k_i the modal stiffness and p_i a modal force.

$$m_i\ddot{q}_i(t) + c_i\dot{q}_i(t) + k_i q_i(t) = p_i(t) \quad \text{with} \quad p_i(t) = \boldsymbol{\psi}_i^T\mathbf{f} \tag{7}$$

The equation can be normalized by the modal mass, so that the coefficients are expressed in terms of natural angular frequencies ω_i and modal damping ratios ζ_i, as they are defined in eq. 8. This leads to eq. 9.

$$\omega_i^2 = k_i/m_i \qquad \text{and} \qquad \zeta_i = \frac{1}{2}\frac{c_i}{\sqrt{k_i m_i}} \tag{8}$$

$$\ddot{q}_i(t) + 2\zeta_i\omega_i\dot{q}_i(t) + \omega_i^2 q_i(t) = \frac{p_i(t)}{m_i} \tag{9}$$

Eq. 9 is an *ordinary differential equation of second order* that has the solution stated in eq. 10 which can be derived by a complex approach where Ω is the excitation frequency. Here, the variable q has already been transformed in the frequency domain which is noted by the circumflex.

$$\hat{q}_i(\Omega) = \frac{1}{\omega_i^2 - \Omega^2 + 2j\zeta_i\omega_i\Omega} \cdot \frac{\hat{p}_i}{m_i} \tag{10}$$

From here the matrix of *frequency response functions* (FRFs) can easily be derived, since the frequency response functions are defined as the displacement response functions multiplied by the inverse of the excitation force vector (eq. 11).

$$\mathbf{H}(\Omega) = \hat{\mathbf{u}}(\Omega)\hat{\mathbf{f}}^{-1}(\Omega) = \sum_{i=1}^{n}\boldsymbol{\psi}_i\hat{q}_i(\Omega)\hat{\mathbf{f}}^{-1}(\Omega) = \sum_{i=1}^{n}\boldsymbol{\psi}_i\frac{1}{\omega_i^2 - \Omega^2 + 2j\zeta_i\omega_i\Omega} \cdot \frac{\boldsymbol{\psi}_i^T}{m_i} \tag{11}$$

For a certain degree of freedom k, the frequency response function due to an excitation force at the l-th degree of freedom can than be calculated by eq. 12.

$$H_{kl}(\Omega) = \sum_{i=1}^{n} \frac{\psi_{ik}\psi_{il}}{m_i\left(\omega_i^2 - \Omega^2 + 2j\zeta_i\omega_i\Omega\right)} \tag{12}$$

If the natural frequencies and damping ratios are known, this equation can be evaluated for discrete excitation frequencies.

3. Experimental Procedures

3.1. Material and Specimens

The goal is to provide the data which is necessary for performing and validating the damage localization approach presented later. Several specimens have been fabricated and have undergone vibration testing in the undamaged and damaged state [13],[14].

Resin-containing carbon-fiber/epoxy prepregs of T300/914 are used to fabricate the test specimens. The material is supplied by Hexcel composites, the physical properties are set out in tab. 1. The specimens are processed in a press. The curing cycle of the laminates is 2h at 180°C with a warming-up cycle of 0.5h at 135°C. The laminates are cut into beams using a diamond wheel cutter, following the ASTM D3039/D3470 standards. The specimens have a thickness of 3mm and consist of 24 plies. The lay-up is chosen as such as the delamination is said to have more profound effects on the dynamic characteristics [25].

Table 1: Properties of pre-impregnated carbon/epoxy T300/914 plies

Property	Symbol	Value
Young's modulus in fibre direction	E_1	$122000MPa$
Young's modulus in transverse direction	E_2	$8500MPa$
Shear modulus	G_{12}	$3570MPa$
Poisson ratios	$\nu_{12}; \nu_{23}; \nu_{31}$	0.25; 0.3; 0.017
Fibre volume ratio		60%
Density	ρ	$1550kg/m^3$
Number of plies		24
Stacking sequence		$[(0/90/45/-45)_3]_s$

The vibration tests are carried out with two steel masses attached at the ends. The aim of putting these masses at the ends is to enhance the difference in the modal parameters between the undamaged and the damaged test specimens [26].

3.2. Vibration Tests

The experimental equipment used for vibration testing is shown in fig. 2b. The experimental set-up is that of a free-free beam excited at its center, based on the *Oberst beam method* [27]. This method states that a free-free beam excited at its center shows the same dynamical behavior as that of a half length cantilever beam. The test specimen is placed centered on a B&K force sensor (type 8200), which is then assembled on a shaker supplied by Prodera, having a maximum

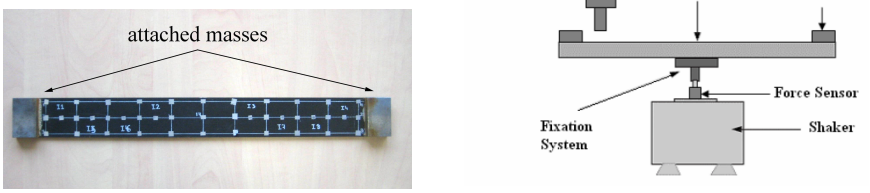

(a) CFRP laminate specimen (b) Experimental set-up for vibration testing

Figure 2: Specimens for vibration testing (a) and schematics of the used Oberst beam test set-up (b). Masses were glued to the ends of the specimens to enhance the change in modal parameters due to damage [26]

force of 100 N. Furthermore, a fixation system is used to connect the test specimens to the force sensor. This fixation is glued to the test specimen with a HBM X60 rapid adhesive. Using a laser vibrometer of type OFV-505, provided by Polytec, the response displacements are measured with high precision and no contact. The shaker, force sensor and the laser vibrometer are manipulated by a data acquisition system running with LMS.Testlab software. Before testing, small reflecting stickers were glued to each of the measurement points on the composite specimens to ensure a good reflection of the vibrometer's laser beam (fig. 2a).

The center of the test specimens is then excited by a *burst random signal*. The excitation point is marked as point 17 in fig. 3. The signal is averaged 10 times for each measurement point and the chosen frequency band is $0-1600Hz$. *Hanning windows* are used for both the output and the input signals. The influence of excitation level is checked and a high frequency resolution ($\Delta f = 0.25Hz$) for precise modal parameter estimation is used. While the level of the excitation signal is chosen as $1N$, the response is measured at 33 points, which are symmetrically spaced in three rows along the length of the beam. The modal parameters are extracted by frequency domain parameter estimation methods (*Polymax*) integrated in the data acquisition system.

The composite beams are analysed in the three different states: An undamaged state (UD), a first damage state due to four impacts (D1) and a second damage state after eight impacts (D2). The locations of the impacts are also shown in fig. 3. Vibration tests are carried out at each of these three states. A simple case is studied where the impact points are chosen as such as the damage is symmetrical on both sides of the two axes of symmetry

After the estimation of the set of frequency response functions, the modal parameters can be determined. This is done by decomposing the frequency response functions into the discrete modes of the system by calculating the poles of the FRF [28]. An enhanced version of this identification is automatically performed by the *LMS.Testlab* software by using the *PolyMAX* method. Tab. 2 shows the experimentally obtained natural frequencies for a composite beam in the undamaged state and for the damage states D1 and D2 after impacts with $8J$.

Furthermore, fig. 4 shows the experimentally obtained frequency response functions for one measurement point on the surface of the composite laminate that has been impacted by $8J$. A remarkable shift in resonances due to impact damage damage can be noticed, especially for higher frequencies.

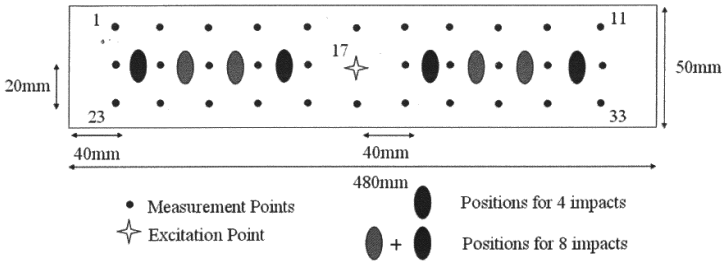

Figure 3: Location of impacts and measurement points on composite beams [13]

Table 2: Estimated resonance frequencies for a composite beam before and after impacting (Impact energy: 8J / PolyMAX method)[13]

	Frequencies [Hz]			
State	1st bending mode	2nd bending mode	3rd bending mode	4th bending mode
undamaged	35.9	284.2	717.0	1416.8
4 Impacts	36.4	279.2	687.9	1363.3
8 Impacts	36.1	270.8	678.7	1236.5

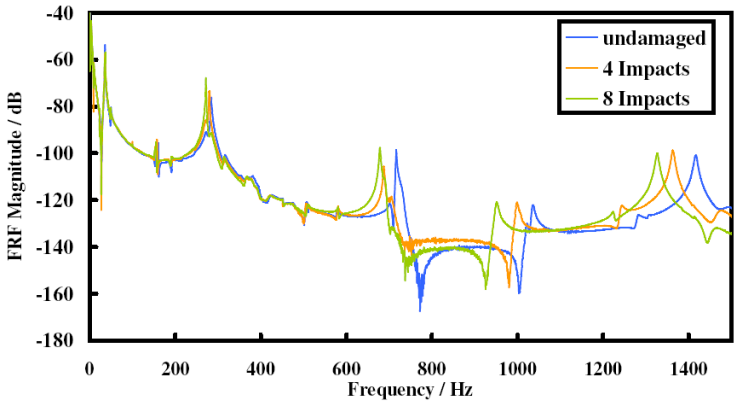

Figure 4: Frequency response functions for point 2 (cp. fig. 3) for a beam impacted with 8J obtained by vibration testing. This figure qualitatively highlights the shifts in resonance frequencies from tab. 2

4. Optimization Problem Formulation for Damage Localization

For formulating general optimization statements suitable for computation, some general definitions have to be established. In the beginning, an objective of the optimization has to be identified as a function of the design variables that are changed in the course of the optimization. Since the principle objective of the performed optimizations is the matching of a set of modal parameters, any kind of matching function (e.g. least square formulations) can be considered. In the present case, due to the nature of the BigDOT optimization algorithm [29], which is based on exterior point penalty functions, a pseudo objective function formulation is constructed where the parameters, which are to be matched, are included as constraints. By the automatic performance of convergence checks for each of the frequency constraints, the number of considered design responses is practically dynamically adapted in every optimization cycle, depending on the fulfillment or non-fulfillment of the constraints. In preliminary tests, this formulation also generally gave more precise results compared to alternative formulations based on finding a search direction from minimizing the least square of all responses together, for example.

Such an exemplary pseudo objective function is shown in eq. 13, where f is the original objective function, and P a penalty function consisting of a set of inequality or equality constraints, which are $\mathbf{g}$ and $\mathbf{h}$, respectively. The parameter r_p is a further penalization coefficient that can be applied to the constraints.

$$\min : \Phi(\boldsymbol{\chi}) = f(\boldsymbol{\chi}) + P(r_p, \mathbf{h}(\boldsymbol{\chi}), \mathbf{g}(\boldsymbol{\chi})) \tag{13}$$

The vector of design variables $\boldsymbol{\chi}$ consists of the Topology design variables corresponding to the *Power Law approach* [22].These design variables are principally an additional element property that can be understood as a relative density of each element e as stated in eq. 14.

$$\chi_e = \frac{\rho_e}{\rho_0} \quad \text{subject to} \quad 0 \leq \chi_{min} \leq \chi \leq 1 \tag{14}$$

Since the variable is normalized by the original densities, it can only assume values between 0 and 1, as stated in the side constraints. Due to numerical reasons, 0 is replaced by a minimum threshold. This design variable is then multiplied by the corresponding element's stiffness and mass and thereby alters the properties of the element (eq. 15).

$$E_e = \chi_e^p E_0 \quad \text{and} \quad m_e = \chi_e^q m_0 \tag{15}$$

The design variable is also penalized, which is supposed to help in getting a clearer *solid-void* solution by making intermediate design variables more "costly". The values of the penalization exponents p and q are problem-dependent, but a penalization factor of about 3 is generally proposed in common literature [30].

In the following, the constraints consisting of modal parameters are defined, where the primed value ($\overline{\omega}$) always denotes the reference data of the damaged structure, and the plain value (ω) corresponds to the current data of the optimized model. Since the goal is to minimize the difference between these values, a proximity ϵ is usually defined. The first set of constraint equations $\mathbf{g}^\omega$ requires the n_ω chosen angular resonance frequencies to be within the proximity ϵ_ω of corresponding resonance frequencies of the damaged structure (eq. 16).

$$g_i^\omega = \left(\omega_i^2 - \overline{\omega}_i^2\right)^2 < \epsilon_\omega \quad \text{for} \quad i = 1, 2, ..., n_\omega \tag{16}$$

This formulation has a global character, since the resonant frequencies are global parameters for the structure. In [20], it is shown that local modal data is necessary for archieving better results, which is why the use of anti-resonances is proposed. Whereas resonances can be found at the peaks of the frequency response functions, their local minima are called anti-resonances (fig. 5). These minima result from the additional contribution of two neighboring modes with a 180 degree phase shift [31]. Anti-resonances are unique for any point on the structure and are therefore considered as local data. The squares of the natural angular frequencies are used for a closer correspondance with the governing equations of this subproblem, namely the undamped system's equations of motion in eq. (2).

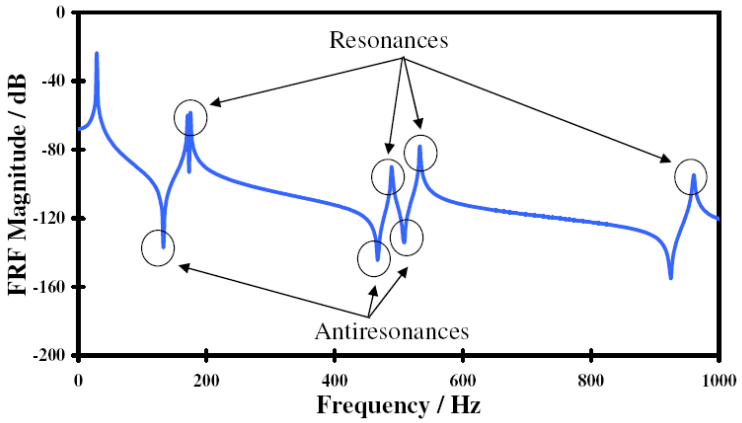

Figure 5: Resonances and anti-resonances in frequency response functions

Due to limitations in *Nastran*, anti-resonances cannot be directly considered as constraints, but nodal frequency response functions, so that anti-resonances can still be included in the optimization by evaluating the FRFs at the corresponding frequency. Thus, the second used set of constraint equations ($\mathbf{g}^H$) requires that the magnitude value of the nodal FRF (FRF of an FE node) at a certain excitation frequency Ω_j is within the proximity of that of the damaged structure at the same frequency (17). As before, the constraints are formulated based on the governing equations in eq. (11). It has however to be noted that the frequency response functions have to be transformed in polar form and only the magnitude is yet used as a constraint.

$$g_j^H = \left(|H_{kl}(\Omega_j)| - |\overline{H}_{kl}(\Omega_j)|\right)^2 < \epsilon_H \quad \text{for} \quad j = 1, 2, ..., n_H \tag{17}$$

Since preliminary simulations with the programmed input file delivered unsatisfying results, a further penalization function is implemented as an additional objective in the optimization. As in these first tests not only the density of the elements in the anticipated region was reduced, but the density of random elements all over the structure, which then led to a unreasonable reduction in global structural mass, the additional function had the objective to penalize the structural mass and thereby guide the optimization towards anticipated results. Furthermore, since the fibre composites do not actually lose mass due to the impacts, it is desired to keep the structural mass close to the original mass, for example. Still, the mass penalization has to be adjusted to the given damage type or material, as shown in the paragraphs dealing with the actual case studies.

Since the design variables are the elements' fractional densities, it is more practical to use also fractional masses for the objective functions, as defined in eq. 18, where m_0 is the mass when the design variables is 1 (*solid*).

$$m_{fractional} = \sum^{n_e} \frac{m_e}{m_0} \tag{18}$$

Here, n_e is the number of elements in the design domain. Due to the constant design volume, this fractional mass is equal to the sum of all fractional densities as shown in eq. 19. Several objective functions have been tested, which are laid out in tab. 3.

$$m_{fractional} = \sum^{n_e} \frac{V_0 \rho_e}{V_0 \rho_0} = \sum^{n_e} \chi_e \tag{19}$$

Table 3: Objective functions for fractional mass penalization

Number	Function	Derivative
(1)	$L = m_{frac}(1 - m_{frac})$	$L' = 1 - 2m_{frac}$
(2)	$L = \|1 - m_{frac}\|$	$L' = -1$ for $m_{frac} < 1$
(3)	$L = (1 - m_{frac})^2$	$L' = -1 + 2m_{frac}$

In fig. 6 it can then be seen that all functions show a relative minimum at the right end of the domain where all fractional densities are 1, but they possess different derivatives, which are important for the sensitivity analysis and basically characterize the penalization. The derivative of function (2) is constant over the whole domain ([0;1]), the derivatives of the other functions are variable with the fractional mass. Whereas the derivative value of function (1) approaches the value of the derivative of function (2) close to the right boarder, the derivative of function (3) approaches zero. Therefore, similar results have been obtained using functions (1) and (2) during the simulations. Also, they generally gave better results than function (3).

4.1. Sensitivity Analysis

Since mathematical programming methods usually involve the calculation of gradients of the objectives for the sensitivity analysis, the derivatives of the constraints with respect to the design variables are presented in this section. Eq. 20 gives the gradients of the resonance frequencies that can be derived from eq. 2 in the frequency domain form as shown in reference [30], where $\boldsymbol{\psi}_{ie}$ and $\boldsymbol{\psi}_{je}$ are the components of the eigenvectors with respect to the nodal degrees of freedom of the element e.

$$\frac{\partial \omega_i^2}{\partial \chi_e} = \boldsymbol{\psi}_{ie}^T \left(\frac{\partial \mathbf{E}_e}{\partial \chi_e} - \omega_i^2 \frac{\partial \mathbf{M}_e}{\partial \chi_e} \right) \boldsymbol{\psi}_{je} \tag{20}$$

The partial derivatives of the frequency response functions have been derived in [32]. Based on eq. 11, the frequency response function can be written as eq. 21.

$$\mathbf{H}(\Omega) = \boldsymbol{\Psi} \hat{\mathbf{q}}(\Omega) \hat{\mathbf{f}}^{-1}(\Omega) \tag{21}$$

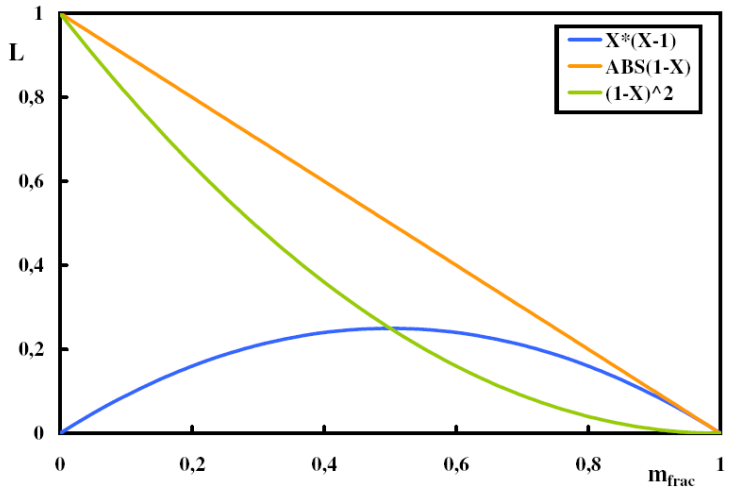

Figure 6: Objective functions for fractional mass penalization (see. tab. 3. Each function posses a relative minimum at $m_{frac} = 1$, that helps to keep the optimization close to the original model

Then, the gradients of the frequency response functions with respect to the element density fraction χ_e are calculated as in eq. 22.

$$\frac{\partial \mathbf{H}(\Omega)}{\partial \chi_e} = \mathbf{\Psi S \hat{q}}(\Omega)\hat{\mathbf{f}}^{-1}(\Omega) \tag{22}$$

Here, $\mathbf{S}$ is the sensitivity matrix as defined in eq. 23, where ω_i is the ith natural frequency and ζ_i the corresponding damping ratio. As before, Ω is the exciting frequency.

$$S_{ij} = \frac{-1}{\omega_i^2 - \Omega^2 + i2\zeta_i\omega_i\Omega}\boldsymbol{\psi}_{ie}^T\left(\frac{\partial \mathbf{E}_e}{\partial \chi_e} - \Omega^2\frac{\partial \mathbf{M}_e}{\partial \chi_e}\right)\boldsymbol{\psi}_{je} \tag{23}$$

In both cases the gradients of the stiffness and mass matrices can be calculated as in eq. 24. These calculations are principally performed in an enhanced form in Nastran.

$$\frac{\partial \mathbf{K}_e}{\partial \chi_e} = \int_{V_e}(\mathbf{DN})^T\frac{\partial \mathbf{E}_e}{\partial \chi_e}\mathbf{DN}dV \qquad \frac{\partial \mathbf{M}_e}{\partial \chi_e} = \int_{V_e}\mathbf{N}^T\frac{\partial \rho_e}{\partial \chi_e}\mathbf{N}dV \tag{24}$$

4.2. Set-up of Topology Optimization Formulation for Damage Localization in Nastran

This section presents the Nastran input file parameters for the damage localization approach. The models that are used for a numerical validation of this method, as well as the modeling of the specimens described in the previous sections are also explained. The latter models are supposed for an experimental validation of the damage localization method.

MD Nastran seemed therefore suitable for an implementation of the localization approach by Lee et al. [20], as with the release of the version *MSC Nastran 2005 r2*, the embedded optimization libraries were enhanced by a topology optimization capability and the introduction of the *BIGDOT* optimizer. Especially this new optimization library provided the capability to

deliver practical results dealing with the large amount of design variables that are common in topology optimization. Thus, only Nastran was available for an "all at once" implementation of the described method combined with low calculation time.

For the optimization of the structure, several new cards have to be added to the input file. At first, the design variable has to be defined. In the case of topology optimization, this is explicitly done by the card TOPVAR. The structure of this card is exemplary shown in tab. 4 with the corresponding symbols from section 4.

Table 4: Definition of Topoloy Optimization variable in Nastran

Command	ID	Label	Type of property	χ_0	χ_{min}	$\Delta\chi$	p	Property ID
TOPVAR	1	DREGION	PSHELL	0.99	0.0001	0.2	3	4

Here, *type of property* characterizes the elements, that are included in the optimization, concerning their deformation behavior. This definition has to be in accordance with the elements of the defined design region, which is called by the *Property ID* that has been assigned prior to the corresponding elements.

Then, the chosen modal parameters of the structure that build up the constraints and objectives have to be included in the calculations. In Nastran, these parameters are referred to *design responses* and they are accessed by the DRESPi entries. For each desired structural response, such a DRESPi entry has to be defined, where the index i denotes the type of design response formulation.

The design responses can then be constrained by referencing the corresponding DRESPi entry in a DCONSTR command and by defining the boundaries there. All the responses and constraints can be called, either by themselves or as a linear combination, by the global objective function (DESOBJ) or the global constraint command DESGLB in the case control section, or, as subcase dependent constraints, by a DESSUB command for each subcase. Figure 7 shows how responses, constraint and objectives can principally be connected. More precise definitions of each of the commands are given in [33] and [34].

In each optimization cycle, two subcases have to be evaluated: the modal analysis and the modal frequency response analysis. Each subcase thereby calls its own set of design constraints via the DESSUB command. An exemplary input file can be found in the appendix A, where the design constraints and corresponding design responses, like the model itself, are sourced out into external files to keep input file mostly model-independent.

4.3. Numerical Modeling

Several numerical models are proposed to test the feasability of the described damage localization method. These models basically consist of two types of specimens, a simple cantilever beam with isotropic material properties for numerical validation and the model of the composite beam for experimental validation.

The procedure for numerical validation is to create an undamaged Finite Element model, copy it and modify the copy by deleting elements at certain points of geometry. This way, a local loss of stiffness can be generated due to the deletion of elements. Modal frequency response analyses are then performed on this template model to obtain the modal parameters of the undamaged and the damaged case. Hereby, the damage localization can be tested on numerical models that lack an experimental base but show sufficient validity for amelioration of

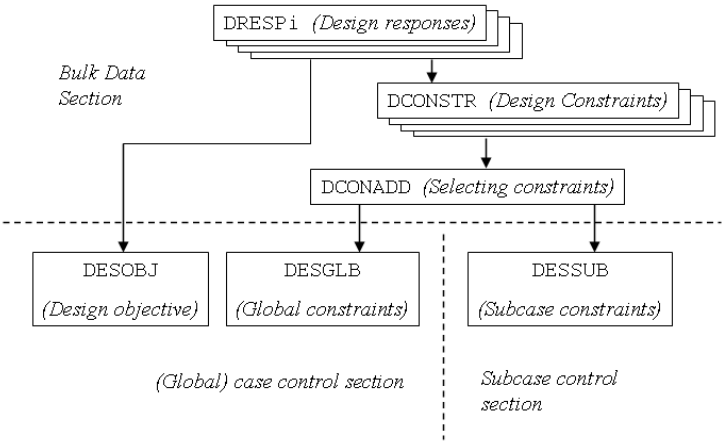

Figure 7: Construction of objective functions and global or subcase design constraints in Nastran input files.

the method prior to the performance of experiments. This process has also been performed in the article by Lee et al. [20].

A cantilever beam test model with homogeneous isotropic material properties is shown in fig. 8a, which was meshed with iso-parametric membrane-bending shell elements. This figure also shows the applied constraints and load. On the free end of the beam a nodal frequency-dependent excitation force with constant amplitude was applied.

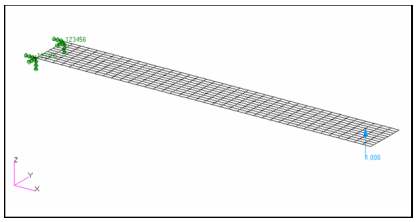

(a) Finite element model of a cantilever beam with applied forces and constraints that has been used as the initial design for preliminary tests of the damage localization method.

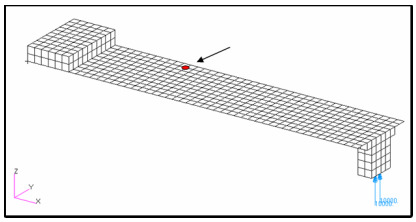

(b) Finite element model for analysed composite beams. The point used for comparison of frequency response functions is marked.

Figure 8

The experimentally tested beams have also been modeled by shell elements. Due to the symmetry of the beams and the vibration test setup, it was sufficient to model only a half beam with the corresponding boundary constraints at the intersection of the the two halves [27]. For the nodes at this intersection the displacements in direction of the excitation force were allowed,

whereas all other degrees of freedom had to be constrained. Furthermore, the connecting piece and the end masses that were glued to the specimens for the vibrations tests had to be explicitely modelled by three-dimensional solid elements. A distributed load with a combined amplitude of $1N$ has been applied to the bottom of the connecting piece to simulate the excitation force of the shaker pot.

Since, at the moment, the topology optimization feature in *Nastran* is still limited to isotropic materials only, the application of the code is also limited to thin quasi-isotropic laminates, for which a plane stress state assumption can be made. Mean stiffnesses can then be calculated based on the laminate theory [1], reducing whole laminate to a two-dimensional shell. Using material properties calculated from such a homogenization of the laminate, the composite beams can be modeled by membrane-bending shell elements as shown in fig. 8b. As mentioned before, damping is not considered in the updating process, since there is no response for damping values implemented in the optmizition module of Nastran. Therefore, a low constant modal damping value of 0,3% has been chosen.

Still, the simple model suceeded to reproduce the dynamic response sufficiently accurate for the present case, since the experimental measured FRF for a randomly chosen point on the surface of the beam fits well with the numerical calculated FRF of the corresponding node (fig. 9).

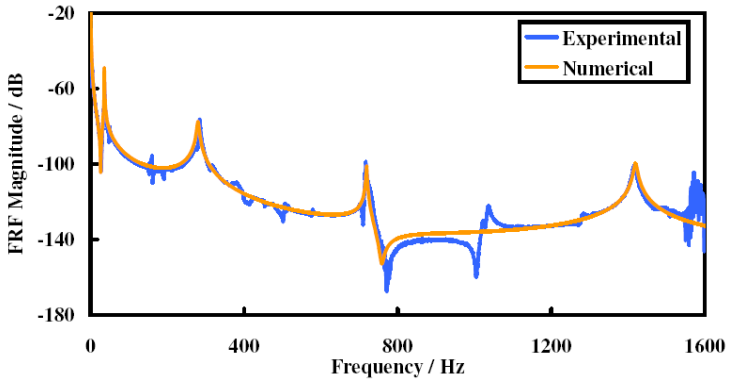

Figure 9: Experimental and numerical estimated frequency response functions of the composite beams for the point marked in fig. 8b.

5. Results and Discussion

5.1. Numerical Validation on Models with isotropic Material Properties

The Nastran input file has then been applied to the described models. Figure 10 shows such an obtained simulation result in terms of the optimized density distribution. Here, the first ten natural frequencies and the resonance and anti-resonance peaks of the FRF at the excitation point in a bandwith from 0 to $500Hz$ were used as matching data. Hereby, the optimization responses were desired to be within a randomly chosen proximity of 5% ($\epsilon < 0.05$) of the target value and the penalization mass was set 97.5%, which is the actual fraction of the number of elements of the damaged to the undamaged structure (ten elements of a total of 400 elements were deleted

for creating the cut out in the damaged template model 10). Although, this test case is based only on numerical models, where the location of damage and the loss in mass was known in advance, the approach can be considered as reproducible with physical specimen. Since, in the actual case of a loss of mass due to impacts in physical specimen, the mass target fraction can be determined by weighing the undamaged and damaged structure. If no difference in mass can be measured, the mass target has simply to be set almost equal to 100%, as it is done with the later presented composite beam.

The density distribution resulting form the optimisation (fig. 10a) is then in quite good concordance with the goal geometry (fig. 10b), since the brighter regions are regions of lower densities that are supposed to represent the damages.

(a)

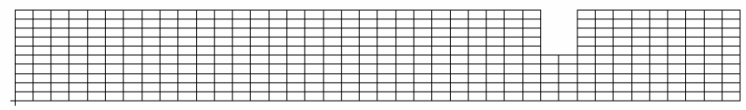

(b)

Figure 10: Results of Topology Optimization on a two-dimensional isotropic model: (a) Resulting density distribution; (b) target model with a cutout.

These result have also been processed by the *imhmax*-function that is available in Matlab and presented in reference [35]. This function supresses all maxima in the intensity image whose heights are less than a threshold, which leads to an even better estimation of damage locations by thresholding the resulting density distribution and supressing false negative damaged regions. The results of the image processing are shown in fig. 11b.

(a) Original results (cp. fig. 10a)

(b) Processed images

Figure 11: Results of Topology Optimization on a two-dimensional isotropic model after processing with the *imhmax*-function provided in Matlab [35]. This function supresses false damage regions and leads a better estimation for damaged regions (fig. 11b)

Furthermore, the frequency response functions and the natural frequencies of the analyzed

model and the target model match very well, as displayed in fig. 12 and tab. 5.

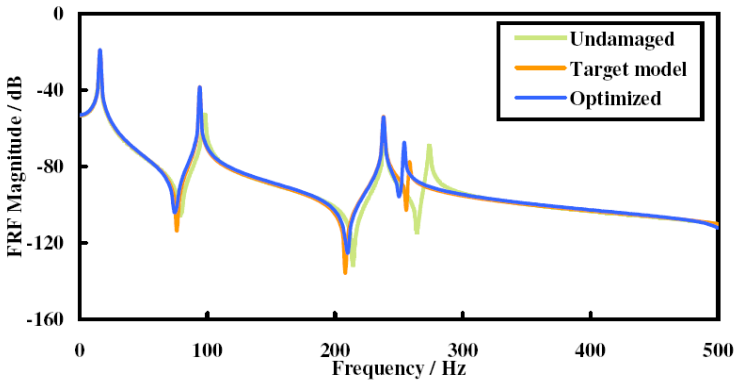

Figure 12: Frequency response functions at the excitation node for the damaged (target) model and the optimization model before and after optimization

Table 5: Natural frequencies of the 2D isotropic test beam with a cutout and the model with optimized density distribution

	Natural Frequencies / Hz	
Mode	Target model	Optimized model
1	16	16
2	94	94
3	238	238
4	256	254
5	257	256
6	513	516

However, the calculation on isotropic materials is performed only for a reproduction of similar results as in [20] and validation of the method's adaption in Nastran. Hereby, the application of this method to localize such evident damage as the cutout in the aluminium beam is not really reasonable, but it becomes all the more interesting when used for localizing non-evident damage in composite beams, as presented in the next sections.

5.2. Experimental Validation on composite beams

The optimization algorithm has then been tried out on the models of the composite specimens. Here, the data used for constraints were the natural frequencies and FRFs that had been obtained by the vibration tests of the damaged specimens (cp. tab. 2 and fig. 4). Since no actual cutout was present, that would justify a penalization mass target as in the numerical validation, the mass target was set to 99%. In the case of the damaged composite specimen, it is reasonable to keep the mass as close the original mass as possible. However, a slight reduction in mass has to be included, allowing some changes in element density and the most suitable mass target value

has yet to be determined depending on the problem, which is a limitation of the method at the moment.

In the following, some Topology Optimization results are presented for the modal parameters of the beam that was impacted with an energy of $8J$. Thereby, two sets of damage state modal parameter data existed for the beams (D1 and D2). Thus, topology optimization was performed with the goal to either localize the first four impact sites or all eight. It has to be reminded, that the beams were considered to be symmetrical, thus each side of the beam has undergone two and four impacts, respectively. The results for the both cases using only resonance frequencies as constraints are shown in fig. 13 and 14 with the corresponding ultra-sound scan.

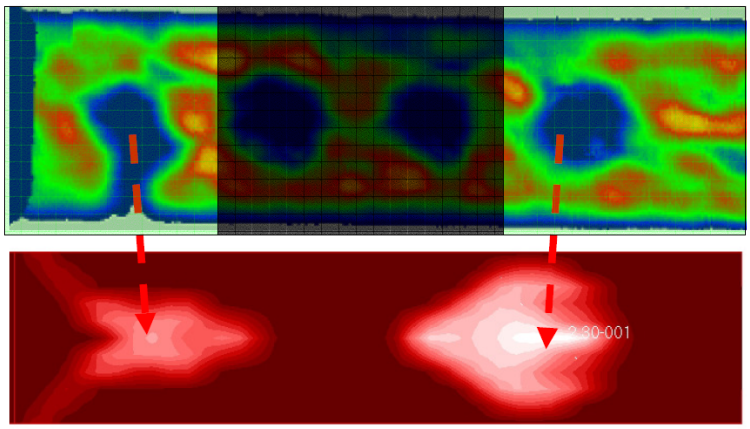

Figure 13: Comparison between C-SCAN results (top) and Damage Localization by TO (bottom) for the damage state D1 - The two middle points are blackened as they correspond to the damage state D2. The applied algorithm is able to easily detect this kind of damage (2 isolated impacts) with high accuracy.

For the first two impacts the right locations have effectively been found with similar sizes as in ultra-sonic images that have been produced after vibration testing (fig. 14; the outer two impact damage sites have been introduced at first (D1), the two inner impacts later (D2, see fig. 3); ultra-sonic testing could only be performed after all other testing had been completed.)

For the more damaged beam with four impact sites only a rather uncertain region of damaged material with lower densities could be located (fig. 14), but not the discrete impact points as shown in the ultra-sound picture, since the damage is very closely spaced and is difficult to differenciate. However, the displayed region of lower densities is still close to a damage region geometry if the delamination regions due to the impacts, that are shown in the ultra-sound image, were merged. Still, for both cases, the FRFs and resonance frequencies show a relatively good match with the damaged cases (fig. 15 and tab. 6).

From the obtained results it can be concluded that their quality depended vastly on the choice of the optimization parameters. These optimization sensitive parameters can be divided in two principle groups. The first on consist of the parameters related to the optimization process, i.e. penalization exponents and objective functions, and the other depends on the set of chosen constraints and quality of the experimental results.

This choice of design constraints is not very intuitive. Since higher resonance frequencies

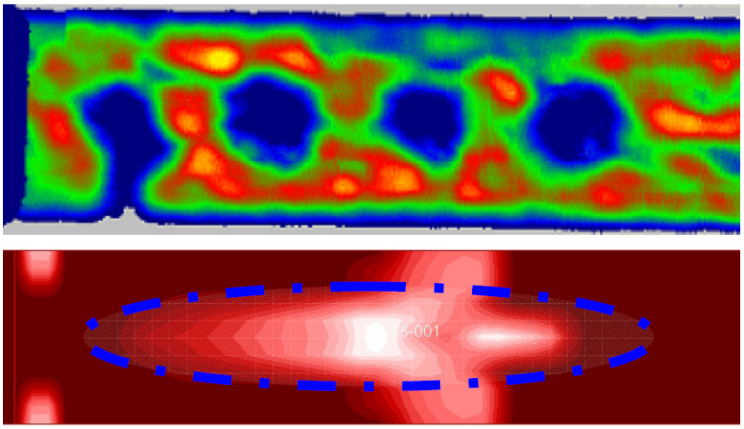

Figure 14: Comparison between C-SCAN results (top) and Damage Localization by TO (bottom) for damage state D2. The developed method highlights here a real limitation: Damage can be detected but it cannot be distinguished between each of the damage sites. The applied algorithm is only capable to show a damage zone delimiting the 4 impacts.

Table 6: Resonance frequencies of tested CFRP beams after 4 and 8 impacts and of the corresponding model with optimized density distribution. Especially the higher frequencies show a relatively good match.

Mode	Frequencies / Hz			
	4 Impacts		8 Impacts	
	Target	Optimization	Target	Optimization
1 (1st bending)	37	30	36	32
2 (2nd bending)	157	148	155	156
3 (3rd bending)	687	679	678	679
4 (4th bending)	1363	1351	1326	1326

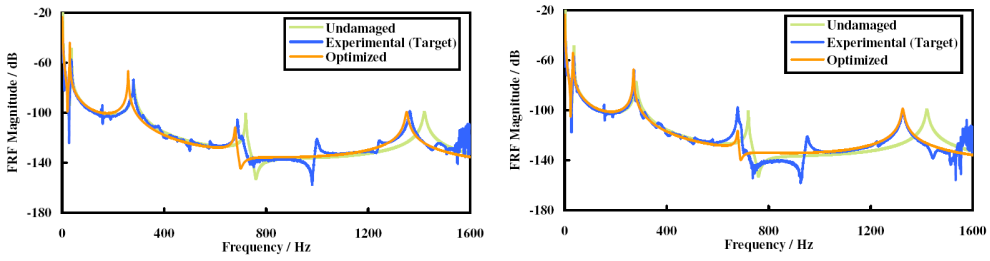

(a) (b)

Figure 15: Experimentally obtained FRF for the composite beams and calculated FRF of the FEM model at the same point (cp. fig. 8b), before and after optimization using only resonance frequency constraints : (a) for 4 impacts; (b) for 8 impacts.

show usually a higher shift due to introduced damages, it seems obvious to use modal parameters of a large spectrum. But with higher frequencies the necessary modal identification becomes more difficult as higher modes are more susceptible to noise and participate less and less in the actual dynamic response.

The presented Topology Optimization approach is also limited to modal parameter shifts due to loss in stiffness and mass, but does not take into account damping, which has proven in experimental results to be more sensitive to damage than stiffness changes ([13],[14],[36]). In the current formulation it is not possible to consider changes in damping as constraints in the optimization, since no direct response for damping is available in *Nastran* so far.

Considering the used optimization algorithm, the implemented BigDOT optimizer in Nastran is an up-to-date algorithm with high efficiency and reliability. Since it is based on mathematical programming, it shows however common problems like possible wrong local optima and is certainly subjected to further developments in numerical optimization. Therefore, for a more detailed validation of the here presented tool, more studies on the optimization parameters and other damage cases are necessary. Still, BigDOT is one of the most capable optimization solutions readily available at the moment and it is especially capable of solving topology optimization problems [29]. Further studies using different optimisation algorithms (stochastic or evolutionary methods, etc.) are encouraged, the principal problem in this damage localisation approach is however still the inclusion of further design responses that are sensitive to damages in the fibre composites.

6. Conclusions

In this paper an enhanced Topology Optimization technique for damage localization is developed based on the works of Lee et al. [20]. In the first part of this paper, the theoretical aspects of this technique are explained, and in the second part, validations of this technique are carried out on numerical models and also composite beams.

The presented damage localization approach can also be divided into two sub-problems, the optimization routine using Topology Optimization and the experimental estimation of modal parameters with the correct numerical modeling.

Concerning the results of the numerical validation, it can be concluded that the feasibility of applying the Topology Optimization approach for damage localization is proven also for an implementation in Nastran. This provides the opportunity for a broader application of the method, especially to more complex structures, that can be more efficiently analyzed in standard industrial finite element codes than in self written codes.

In the process of experimental validation, we succeed in localizing seperate damage zones, but the results become less clear and the optimization might get stuck in wrong local optima regarding the results of C-Scans of the specimens. But it can be assumed, that the poor results for the D2 damage case follow from the simplistic modeling, the lack of constraint data and not taking into account damping changes, rather than due to a conceptional error in the approach. Still, with a suitable choice of parameters, some good results with correct localization of the impacts on the composite beams can be archieved.

However, the approach has yet only been validated for one composite laminate beam. In the near future, this study shall be extended to all the other composite beams tested in reference [14]. The approach shall also be applied to localizing damage in standard sandwich specimens with honeycomb and foam cores, as C-Scan testing is not very capable of detecting damage in composite sandwiches. Further prospects of this work could be an optimization using more design

responses, like directly addressing the mentioned anti-resonances or mode shapes by referencing the imaginary part of the FRFs, and to increase the analysed frequency bandwidth to take into account higher modes.

Acknowledgements

The authors gladly thank PhD student Thibault Gouache for his contributions to this article and to the structural dynamics work group of the ISAE Toulouse.

Appendix

A. Nastran Input File for Damage Localization by Topology Optimization

This Nastran input file can generally be applied to finite element models when the correct model geometry and optimization constraints are included and the commented parameters are adjusted.

```
$--------File Managementsection-----------------------
$--------Executive Control Section--------------------
SOL 200
TIME 20
CEND
$--------Global Case Control Section------------------
TITLE = Damage localization
ECHO = NONE
$--SOL 200 specific Parameters:
MAXLINES = 999999
SET 1 = 101 $ Excitation Loadset
SET 2 = 459,254 $ Nodes to be included in Calculation
DESOBJ = 201 $ Design Object referencing a Design Response
$---------------Subcases-------------------------------
SUBCASE 1
$--Name of Subcase:
   SUBTITLE = Modal Analysis
   ANALYSIS = MODES
   METHOD = 1                   $ Lanczos method
   SPC = 2
   DESSUB = 300                 $ Set of design constraints associated with natural frequencies
   DRSPAN = 1                   $ FRMASS response calculation
SUBCASE 2
$--Name of Subcase:
   SUBTITLE = Frequency Response
   ANALYSIS = MFREQ             $ Modal frequency response analysis
   METHOD = 1
   FREQUENCY = 1                $ Frequency table for FRF calculation
   SPC = 2
   DLOAD = 2
   LOADSET = 4
   SDAMPING = 1                 $ Damping included
   DISP(PHASE) = 2
   DESSUB = 320                 $ Set of Design Constraints FRF Data
$---------------Bulk Data Section--------------------
BEGIN BULK
$---------------Parameters----------------------------
PARAM   POST    0
PARAM   PRTMAXIM YES
$--FE Analysis related parameters:
PARAM   RESVEC  YES
$--Optmization related parameters:
PARAM   DESPCH   10
$--Frequency table for FRF calculations
FREQ1   1       0.      1.      1600
```

```
$--Table for modal damping ratios
TABDMP1 1       CRIT
        0.      0.003   1600.   0.003   ENDT
$--Eigenvalue extraction table
EIGRL   1                       20      0
$---------------Geometry-------------------------------
$--Include Model file here (*.bdf)
INCLUDE 'modelgeometry.bdf'
$---------------BCs------------------------------------
$--referencing BCs in geometry file
SPCADD   2       1
$---------------LOADs----------------------------------
$--referencing Loads in geometry file
RLOAD1   3       5                       1
LSEQ     4       5       1
DLOAD    2      1.      1.      3
$--Frequency dependent load amplitude
TABLED1  1
         0.      1.      1600.   1.      ENDT
$---------------Further Parameters---------------------
$--Topoly Optimisation Variable
$--(Choice of correct design domain!)
TOPVAR  1       PSHELL  PSHELL  0.99    .0001   .3      2.      4
$--Include optimization constraints file here
INCLUDE 'optimizationconstraints.bdf'
$--Objective Function
DRESP1   101     OBJ     FRMASS
DRESP2   201     EQART   401
         DRESP1  101
$--Objective Functions
$ 1
$DEQATN   401     F1(X)=0.99*X-X**2
$ 2
DEQATN   401     F1(X)=ABS(0.99-X)
$ 3
$DEQATN   401     F1(X)=(0.99-X)**2
$--Optimisation Parameters
DOPTPRM CONV1   .001    DESMAX   50     CONVDV  1e-6    CONVPR  1e-6
$--------------End------------------------------------
ENDDATA
```

References

[1] S. W. Tsai, H. T. Hahn, Introduction to Composite Materials, Technomic, Lancaster, Pennsylvania, 1980.

[2] M. Y. Kashtalyan, C. Soutis, Mechanisms of internal damage and their effect on the behavior and properties of cross-ply composite laminates, International Applied Mechanics 38 (6) (2002) 3–22.

[3] M. Gude, W. Hufenbach, I. Koch, R. Protz, Fatigue failure criteria and degradation ruls for composites under multiaxial loadings, Mechanics of Composite Materials 42 (5) (2006) 631–641.

[4] V. Li, T. Kanda, Z. Lin, Influence of fibre/matrix interface properties on complementary energy and composite damage tolerance, Key Engineering Materials 145 (1998) 465.

[5] R. M. Gadelrab, The effect of delamination on the natural frequencies of a laminated composite beam, Journal of Sound and Vibration 197 (3) (1996) 172–181.

[6] Y. Yan, L. Cheng, Z. Wu, L. Yam, Development in vibration-based structural damage detection technique, Mechanical Systems and Signal Processing 21 (2007) 2198–2211.

[7] S. W. Doebling, C. R. Farrar, M. B. Prime, D. W. Shevitz, Damage identification and health monitoring of structural and mechanical systems from changes in their vibration characteristics: A literature review, Tech. rep., Research Report LA-13070-MS Los Alamos National Laboratory (1996).

[8] Y. Zou, L. Tong, G. P. Steven, Vibration-based model-dependent damage (delamination) identification and health monitoring for composite structures - a review, Journal of Sound and Vibration 230 (2) (2000) 357–378.

[9] S. W. Doebling, C. R. Farrar, M. B. Prime, A summary review of vibration-based damage identification methods, Tech. rep., Los Alamos National Laboratory (1998).

[10] H. Sohn, C. Farrar, F. Hemez, D. Shunk, D. Stinemates, B. Nadler, A review of structural health monitoring literature, Tech. rep., Los Alamos National Laboratory Report LA-13976-MS. (2001).

[11] E. Carden, P. Fanning, Vibration based condition monitoring: A review, Structural Health Monitoring 3 (4) (2004) 355–377.
[12] B. Schwarz, M. M.H Richardson, Experimental modal analysis, in: CSI Reliability week, Orlando FL, 1999.
[13] A. Shahdin, J. Morlier, Y. Gourinat, Correlating low energy impact damage with changes in modal parameters: A preliminary study on composite beams., Accepted January 09 in Structural Health Monitoring.
[14] A. Shahdin, J. Morlier, Y. Gourinat, Significance of low energy impact damage on modal parameters of composite beams by design of experiments, Accepted in 7th International Conference on Modern Practice in Stress and Vibration Analysis, MPSVA 2009.
[15] J. Tracy, G. Pardoen, Effect of delamination on the natural frequencies of composite laminates, Journal of Composite Materials 23 (12) (1989) 1200–1215.
[16] R. D. Adams, R. Cawley, The localization of defects in structures from measurements of natural frequencies, Journal of Strain Analysis 14 (1979) 49–57.
[17] M. H. Richardson, M. A. Mannan, Correlating minute structural faults with changes in modal parameters, Proceedings of Spie, International Societe of Optical Engineering 1923 (2) (1993) 893–898.
[18] O. Salawu, Detection of structural damage through changes in frequency: a review, Engineering Structures 19 (9) (1996) 718–723.
[19] Z. Zhang, G. Hartwig, Relation of damping and fatigue damage of unidirectional fibre composites, International Journal of Fatigue 24 (2004) 713–738.
[20] J. S. Lee, J. E. Kim, Y. Y. Kim, Damage detection by the topology design formulation using modal parameters, International Journal for Numerical Methods in Engineering 69 (2007) 1480–1498.
[21] M. P. Bendsoe, N. Kikuchi, Generating optimal topologies in structural design using a homogenization method, Computer Methods in Applied Mechanics in Engineering 35 (1992) 1487–1502.
[22] M. Bendsoe, Optimal shape design as a material distribution problem, Structural Optimization 1 (1989) 193–202.
[23] D. J. Ewins, Modal Testing: Theory, Practice and Applications, 1984.
[24] M. Hörnlund, A. Papazoglu, Analysis and measurments of vehicle door stru dynamic response, Master's thesis, Division of Structural Mechanics, LTH, Lund University, Sweden (2005).
[25] D. Saravanos, D.A.Hopkins, Effects of delaminations on the damped dynamic characteristics of composites, Journal of Sound and Vibration 192 (1995) 977–993.
[26] K. Vanhoenacker, J. Schoukens, P. Guillaume, S. Vanlanduit, The use of multisine excitations to characterise damage in structures, Mechanical Systems and Signal Processing 18 (2004) 43–57.
[27] J. L. Wojtowicki, L. Jaouen, New approach for measurements of damping properties of materials using oberst beams, Review of Scientific Instruments 75 (8) (2004) 2569–2574.
[28] D. L. . Brown, R. J. Allemang, R. Zimmermann, M. Mergeay, Parameter estimation techniques for modal analysis, Society of Automotive Engineers Paper No. 790221.
[29] G. Vanderplaats, Very large scale optimization, Tech. Rep. NASA/CR-2002-211768, Vanderplaats Research and Development, Inc., Colorado Springs, Colorado (2002).
[30] M. P. Bendsoe, O. Sigmund, Topology Optimization - Theory, Methods and Applications, Springer Verlag, 2003.
[31] P. Avitabile, Experimental modal analysis - a simpel non-mathematical presentation, Sound and Vibration 35 (1) (2001) 20–31.
[32] Z.-D. Ma, N. Kikuchi, I. Hagiwara, Structural topology and shape optimization for a frequency response problem, Computational Mechanics 13 (1993) 157–174.
[33] MSC.Software Corporation, Santa Ana, CA, USA, MSC Nastran 2007 r1 - Users Guide for Topology Optimization, r1 Edition (2007).
[34] MSC.Software Corporation, Santa Ana, CA, USA, MSC Nastran 2007 Quick Reference Quide (2007).
[35] P. Soille, Morphological Image Analysis: Principles and Applications, Springer Verlag, 1999.
[36] D. Montalvão, N. Maia, A. Ribeiro, A review of vibration-based structural health monitoring with special emphasis on composite materials, The Shock and Vibration Digest 38 (4).